THE JOURNAL OF PHYSICAL CHEMISTRY A
A JOURNAL OF THE AMERICAN CHEMICAL SOCIETY

pubs.acs.org/JPCA

Article

The Molecular and Electronic Structure of $NdF_2^{-/0}$

Burak A. Tufekci, Isuru R. Ariyarathna,* Kathryn Foreman, and Kit H. Bowen*

Cite This: https://doi.org/10.1021/acs.jpca.6c01401

Read Online

ACCESS | Metrics & More | Article Recommendations | Supporting Information

ABSTRACT: The molecular and electronic structures of NdF_2^- and NdF_2 were elucidated through a combined anion photoelectron spectroscopy and quantum chemistry investigation. The anion photoelectron spectrum of NdF_2^- yielded an experimental vertical detachment energy (VDE) of 1.11 eV, in excellent agreement with the theoretical estimate of 1.106 eV. The calculated adiabatic electron affinity (AEA) of 1.055 eV lies close to the VDE, consistent with the similar optimized structures of the anion and neutral. Geometry optimizations confirm that both NdF_2^- and NdF_2 adopt bent C_{2v} structures with the anion possessing a $^4A_2$ ($4f^36s^2$) ground state and the neutral possessing a $^5A_2$ ($4f^36s^1$) ground state. Extensive multireference calculations reveal a dense manifold of low-lying neutral excited states. Moreover, we juxtapose $NdF_2^{-/0}$ with its periodic analogue $UF_2^{-/0}$, showing similar metal-centered s-electron photodetachment, bent anion/neutral structures, and largely nonbonding 4f/5f electrons. Together, these results demonstrate the collaborative utilization of aPES with relativistic multireference calculations for the electronic structure of f-element molecules.

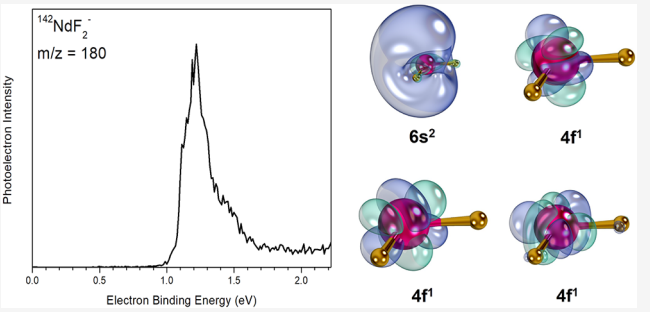

INTRODUCTION

While the rare earths are not truly "rare" in terms of their natural abundance, their unique physicochemical properties make them essential in niche applications such as batteries, catalysis, magnets, ceramic additives, and high-temperature coatings.[1] Such applications of the rare earths have ultimately led the market to grow to $9.6 billion by 2026, at a 12.3% compound annual growth rate.[2] What makes them "rare" is the difficulty in their separation, rather than their actual scarcity.[3] In particular, Nd and La are produced by an effective and low cost method of molten salt electrolysis, which uses halogen containing electrolytes, specifically that of chloride and fluoride.[4−6] Among the rare earth elements (REEs), however, neodymium stands out for its exceptional magnetic properties, hydrogen absorption capabilities, and catalytic activity.[1,7]

Separating the lanthanides remains a significant challenge. The primary techniques: chemical separations, fractional crystallization, ion-exchange, and solvent extraction are laborious and expensive. Of these, solvent extraction is the most widely used on an industrial scale, with the exception of cerium.[8] While relatively efficient for rare earth elements with significant differences in their ionic radii, solvent extraction becomes increasingly difficult as a result of the *lanthanide contraction*. The lanthanide contraction is a trend that results in the decrease in the radius of the lanthanide ion Ln^{3+} along the row. Due to the three angular nodes of the 4f orbitals, the 5s and 5p orbitals become poorly shielded, which results in those valence orbitals becoming more core-like than expected.[9] This contraction not only gives rise to minimal participation of bonding from 4f electrons, but causes the latter lanthanides to have nearly identical properties, which requires multiple extraction steps in order to achieve high purity.[8,10,11] Ultimately, it is the large number of low-lying *molecular* electronic states, which arise from the radial density of the 4f orbitals being "dug deep" inside the 5s-5p core, high angular momentum from the 4f electrons, and spin multiplicity of low-lying electronic states with partially filled 4f, 5d, and 6s orbitals, that makes elucidating the electronic structure of lanthanide-containing diatomic and polyatomic molecules so difficult.[12]

Regardless, understanding how 4f/5f-electrons participate in chemical bonding remains a central topic in developing a unified description of heavy-element chemistry. Unlike the relatively compact 4f orbitals, the 5f orbitals possess a radial node making them more spatially extended, implying a greater propensity for bonding. In the periodic table, elements in the same column (group) share similar degrees of valency and often exhibit similar physicochemical properties. Hence, the periodicity warrants a direct comparison of lanthanides (4f systems) to actinides (5f systems). For neodymium (Nd, $[Xe]4f^46s^2$) the actinide analogue is Uranium (U, $[Rn]-5f^36d^17s^2$), which lies directly below it on the periodic table

Received: March 2, 2026
Revised: June 16, 2026
Accepted: June 19, 2026

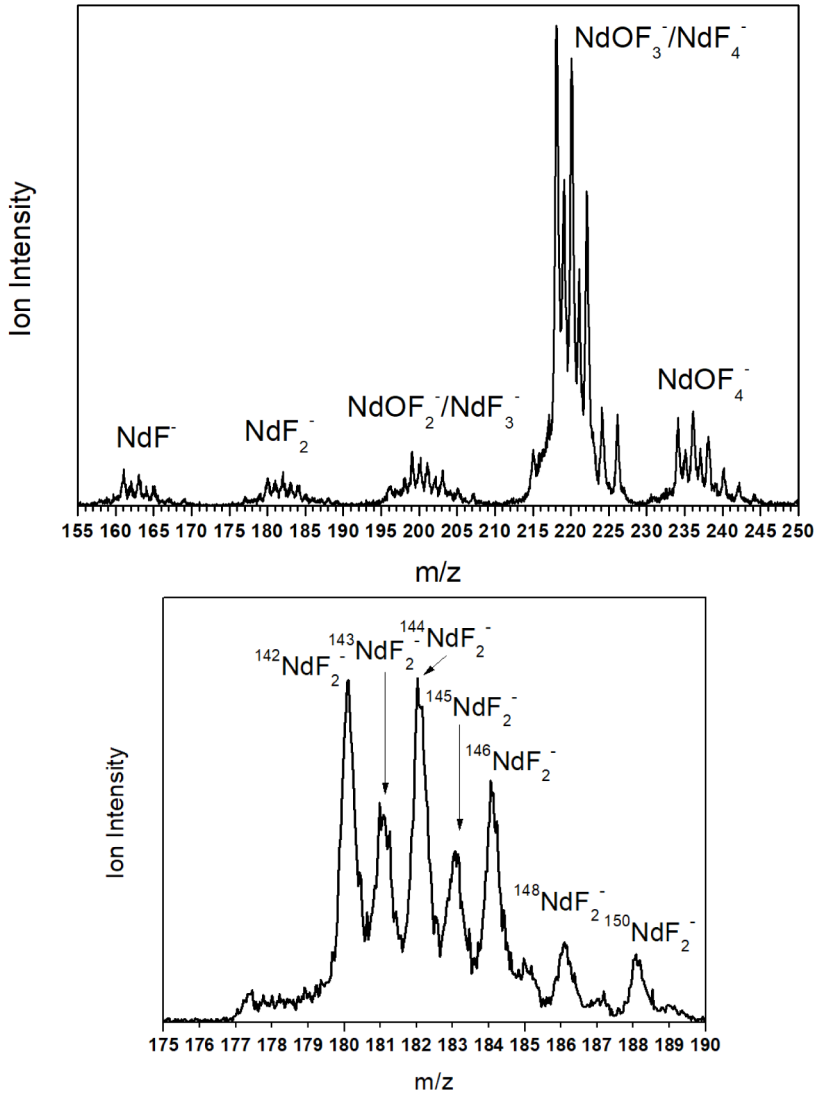

Figure 1. Mass spectrum from the laser ablation of a Nd rod in the presence of anhydrous HF. Zoomed in spectrum of NdF_2^- (bottom).

and possesses a diffuse set of three 5f electrons. While Nd commonly adopts the +III oxidation state, U can have oxidation states spanning from +III to +VI, with +IV and +VI being the most stable. Nevertheless, periodicity alone does not predict bonding trends in the heavy elements, where relativistic effects are substantial and cannot be overlooked.

In this work, we test the concept of periodicity while accounting for relativistic effects by taking the experimental anion photoelectron spectrum of NdF_2^-, a 4f molecular system, and juxtaposing it with its analogous, and previously published, 5f system, UF_2^-.[13] We complement the experiment with relativistic, high-level ab initio calculations that reproduce the spectral energies and assign underlying electronic states, enabling analysis of orbital contributions and covalency in the M-F bonds. As expected, the 4f orbitals do not appreciably participate in the bonding of $NdF_2^{-/0}$, yet this synergistic effort maps out the electronic and molecular structure of $NdF_2^{-/0}$ in detail and provides benchmarks for future computational methodology in heavy-element chemistry.

EXPERIMENTAL METHODS

The anion source and anion photoelectron spectrometer has been described in a previous paper.[14] Briefly, NdF_{1-4}^- anions were generated by ablating a Nd rod by laser vaporization (LVS), while being backed by a ~1% HF in He carrier gas mixture. The carrier gas mixture is adiabatically expanded into high vacuum, which promotes cooling and potential clustering of the hot anions generated from the laser ablation process. Figure 1 shows that Nd has multiple isotopes, so it was necessary to mass filter the anions of interest before photodetachment in order to prevent mass contamination in the aPES. The anions were then mass analyzed with our Wiley−McLaren time-of-flight mass spectrometer (TOFMS), where they were also mass-selected, and momentum-decelerated prior to photodetachment by 532 nm (2.33 eV) wavelength photons. The electron kinetic energies (EKEs) of the photodetached electrons were energy analyzed by a magnetic bottle photoelectron spectrometer. The electron binding energy (EBE) was then calculated using the relationship $hv = EKE + EBE$, where hv is the energy of the photons used for photodetachment. The resultant 532 nm anion photoelectron spectrum was calibrated with Pb^-.[15]

COMPUTATIONAL METHODS

Density functional theory (DFT) calculations were performed using the Gaussian 16[34] software suite. For DFT calculations, default SCF (self-consistent field) convergence thresholds and grids available in Gaussian 16 were applied. The global generalized gradient approximations hybrid B3LYP[16,17] density functional approximation was used for DFT calculations. The DFT/B3LYP geometry

https://doi.org/10.1021/acs.jpca.6c01401
J. Phys. Chem. A XXXX, XXX, XXX−XXX

optimizations and harmonic vibrational frequency calculations were performed with aug-cc-pVQZ[18] basis set of F and Stuttgart relativistic small-core (RSC) 1997 quadruple-ζ basis set with a 28-electron effective core potential (28 ECP) of Nd.[19,20] The optimized wave functions were used for all DFT calculations by executing stable = opt option in Gaussian 16.[1]

For multireference calculations MOLPRO 2023.2[21,22] code was used. All multireference calculations were performed under C_{2v} symmetry. First, the quartet-spin DFT/B3LYP geometry was used as an approximate starting structure for complete active space second-order perturbation theory (CASPT2) geometry optimizations of 1^4A_1, 1^4B_1, 1^4B_2, and 1^4A_2 states of NdF_2^-. For these calculations, cc-pVDZ-DK3 (Nd)[23] aug-cc-pVDZ-DK (F)[24,25] correlation consistent basis set was used with the third-order Douglas-Kroll-Hess (DKH) Hamiltonian. For all CASPT2 calculations an imaginary shift of 0.02 and ionization potential electron affinity of 0.3 were applied. Using the same method, geometries of the most stable 1^4A_2 of NdF_2^- and 1^5A_1, 1^5B_1, 1^5B_2, 1^5A_2 states of NdF_2 were optimized at the at the large cc-pVTZ-DK3 (Nd) aug-cc-pVTZ-DK (F) basis set (hereafter ATZ). At the CASPT2 level, vertical electron detachment energy of NdF_2^- were calculated using the ATZ basis set as well as the larger cc-pVTZ-DK3 (Nd)[23] d-aug-cc-pVTZ-DK (F)[24−27] basis set. Hereafter cc-pVTZ-DK3 (Nd) d-aug-cc-pVTZ-DK (F) basis set combination is denoted by DATZ. For VDE calculations ATZ-CASPT2 geometry of NdF_2^- (1^4A_2) was used. The same geometry was used to perform multireference configuration interaction (MRCI)[28−30] excited state calculations of NdF_2 under the ATZ basis set. The ATZ-CASPT2 geometries of NdF_2 (1^5A_2) and NdF_2^- (1^4A_2) were used to obtain the adiabatic electron attachment energy (AEA) of NdF_2. Davidson relaxed correction (MRCI+Q)[31] was applied to evaluate the approximate quadruple substitution-like effect. The spin−orbit calculations of NdF_2 were carried out at the ATZ-MRCI+Q level using the Breit-Pauli Hamiltonian as implemented in MOLPRO. In the spin−orbit calculations, the MRCI energies in the diagonal elements were replaced with MRCI+Q energies. All MRCI and CASPT2 calculations of NdF_2^- and NdF_2 were performed on top of complete active space self-consistent filed (CASSCF)[32−35] wave functions produced by CAS(5,11) (5 electrons in 11 orbitals) and CAS(4,11) active spaces, respectively. The 11 orbitals correspond to the 6s, seven 4f, and three 5d orbitals of Nd. At the MRCI and CASPT2 levels all valence electrons were correlated.

RESULTS AND DISCUSSION

Due to the presence of multiple naturally occurring isotopes of neodymium, mass selection was critical to ensure that no mass-coincident species were unintentionally photodetached. In addition to the aPES spectrum of $^{142}NdF_2^-$ at m/z = 180, the aPES spectrum of $^{150}NdF_2^-$ was also collected to verify the consistency of the electronic structure among isotopes (Figure S1). The lowest electron-binding-energy (EBE) peak labeled X in the aPES of NdF_2^- shown in Figure 2 is assigned as the experimental vertical detachment energy (VDE), which was determined to be 1.11 eV. Similarly, in the previously reported UF_2^- spectrum, the low-EBE feature X' was assigned as the experimental VDE at 1.18 eV. In both cases, the determined VDE transition is not necessarily the most intense peak in the spectrum. This assignment is further supported by the structural similarities between $UF_2^{-/0}$ and $NdF_2^{-/0}$. Both UF_2^- and UF_2 are bent C_{2v} species, and upon photodetachment the U−F bond length decreases slightly from 2.092 Å to 2.054 Å, while the F−U−F angle changes from 105.2° to 101.7°. Analogously, NdF_2^- and NdF_2 are also bent C_{2v} species with similar anion and neutral ground-state structures, where the Nd−F bond length changes from 2.074 Å to 2.032 Å and the F−Nd−F angle changes from 110.7° to 114.6°. The electron affinity (EA) transition corresponds to the adiabatic energy difference between the respective optimized anion and neutral ground-state structures, whereas the VDE corresponds to photodetachment to the neutral at the fixed equilibrium geometry of the anion. Therefore, in both molecular systems, because the structures of the anion and neutral are similar, the EA- and VDE- determining transitions can be expected to occur at nearly the same EBE, supporting the assignments of peaks X and X' as the VDEs of NdF_2^- and UF_2^-, respectively. In addition, in the spectrum of NdF_2^-, peaks adjacent to the VDE indicate a vibrational progression, with a rough spacing of ~40 meV. Notably, the NdF_2^- spectrum has a shoulder on the high EBE side similar to that reported for UF_2^-, further suggesting analogous photodetachment processes in the two systems.

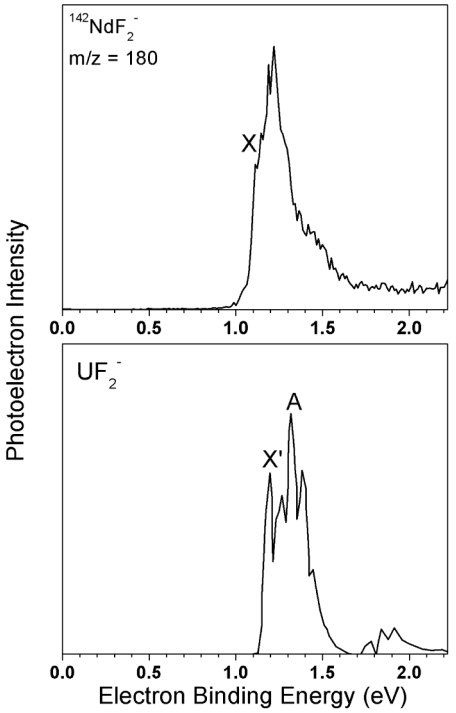

Figure 2. Anion photoelectron spectrum of $^{142}NdF_2^-$ (top) compared to the spectrum of UF_2^- (bottom).[13]

We used DFT/B3LYP to investigate the geometries and their harmonic vibrational frequencies of different spins of NdF_2^- and NdF_2 aiming to confirm their stability on the potential energy surface. Our DFT/B3LYP findings are listed in the ESI Tables S1 and S2. DFT/B3LYP predicted a quartet-spin ground state for the NdF_2^- with an energetically closely lying sextet-spin structure (~0.3 eV). We found that its doublet- and octet-spin structures are as high as 1.2 and 7.45 eV respectively compared to the ground quartet-spin structure. The same level of theory predicted a quintet-spin ground state for the NdF_2 molecule and a triplet-spin excited structure at ~0.5 eV above. Its singlet- and septet-spin excited states were predicted to be at ~1.5 and 5.6 eV above. Even though the single-reference DFT/B3LYP is known to provide reasonably accurate results on molecular complexes, the *ab initio* multireference wave function theories are the unanimous choice for investigating highly correlated complexes such as NdF_2^- and NdF_2. Hence, we have analyzed the quartet-spin NdF_2^- and quintet-spin NdF_2 species at the multireference CASPT2 level of theory. Our CASPT2 findings are reported in the ESI Tables S3 and S4. Since 1^4A_1, 1^4B_1, 1^4B_2, 1^4A_2 of NdF_2^- and 1^5A_1, 1^5B_1, 1^5B_2, 1^5A_2 of NdF_2 lie very close in

https://doi.org/10.1021/acs.jpca.6c01401
J. Phys. Chem. A XXXX, XXX, XXX−XXX

energy, it is rather difficult to precisely declare their ground state symmetries. However, based on the CASPT2 predictions the most stable structures of NdF_2^- and NdF_2 are $^4A_2$ and $^5A_2$, respectively.

The NdF_2^- (1^4A_2) bears $4f^36s^2$ electronic configuration with the multireference composition of $0.80[(1a_1)^2(2a_1)^1(1b_1)^1(1b_2)^1] - 0.39[(1a_1)^2(1b_1)^1(2b_1)^1(1a_2)^1]$ (the corresponding molecular orbitals are given in Figure 3).

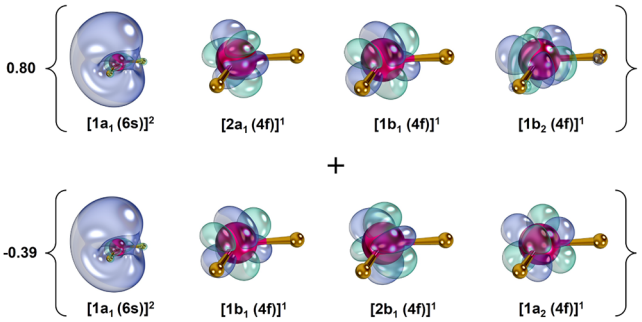

Figure 3. Two dominant configurations of the NdF_2^- (1^4A_2). The illustrated CASSCF orbitals were produced using the IboView[36] software. Nd and F atoms of each orbital plot are shown in magenta and gold spheres, respectively. The two phases of orbitals are shown in blue and green.

The removal of an electron from the $6s^2$ of Nd of NdF_2^- ($^4A_2$) creates the NdF_2 ($^5A_2$). This parallels the photodetachment of UF_2^-, which corresponds to the removal of a 7s electron.[13] Likewise, for UF_2^- the electron configuration is $5f^37s^2$ and neutral UF_2 has a $5f^37s^1$ configuration, highlighting the similar electronic structures ($f^3s^2 \rightarrow f^3s^1$) and s-electron detachment.

Furthermore, similar to NdF_2^- (1^4A_2), NdF_2 (1^5A_2) carries multireference characteristics with slightly different coefficients (i.e., $0.83[(1a_1)^1(2a_1)^1(1b_1)^1(1b_2)^1] - 0.49[(1a_1)^1(1b_1)^1(2b_1)^1(1a_2)^1]$). Even though the ground states of NdF_2^- (1^4A_2) and NdF_2 (1^5A_2) bear some multireference characters, our multireference CASPT2 and single-reference DFT/B3LYP methods predicted similar geometries. Specifically, the CASPT2 r_e (Nd−F lengths in Å) and α (F−Nd−F angle in degrees) of NdF_2^- (1^4A_2) and NdF_2 (1^5A_2) are [2.074, 110.7] and [2.032, 114.6], whereas the corresponding DFT/B3LYP values are [2.120, 112.1] and [2.035, 112.7], respectively. The ATZ-CASPT2 level predicted a 0.998 eV adiabatic electron attachment [AEA: $\Delta E(^5A_2$ of $NdF_2 - {}^4A_2$ of $NdF_2^-)$] energy for the NdF_2 molecule. However, DFT/B3LYP underestimated the AEA of NdF_2 by ∼2% (i.e., DFT/B3LYP AEA of NdF_2 is 0.763 eV). The significant discrepancy between CASPT2 versus DFT/B3LYP could be due to the DFT/B3LYP method's inadequacy in predicting energetics of multireference systems.

We have considered the 1^5A_2 of NdF_2 and 1^4A_2 of NdF_2^- to calculate the VDE of NdF_2^-. The ATZ-CASPT2 VDE of NdF_2^- is 1.038 eV. The correlation of $5s^25p^6$ electrons of Nd at the ATZ-CASPT2 level (ATZ-C-CASPT2) increased the VDE to 1.081 eV. The improvement of the basis set from ATZ to DATZ further increased the VDE to 1.096 eV (DATZ-C-CASPT2). However, the spin−orbit effects of small lanthanide-based molecular species are known to be significant and must be accounted for in order to obtain accurate VDE values. We attempted to perform spin−orbit calculations under the ATZ-CASPT2 level but due to the convergence issues that arose, we adopted MRCI and MRCI+Q levels for calculating spin−orbit effects on VDE and excitation energies. The spin−orbit effects disregarded ATZ-MRCI and ATZ-MRCI+Q VDE values of NdF_2^- are 0.948 and 0.983 eV respectively and are in good agreement with the ATZ-CASPT2 value. The spin−orbit coupling effects of NdF_2 and NdF_2^- are each approximately 0.4 eV, with only a 0.004 eV impact on the VDE. The spin−orbit effects accounted ATZ-MRCI+Q VDE of NdF_2^- is 0.987 eV. By adding this spin−orbit correction and the zero-point energy correction (obtained at DFT/B3LYP; 0.006 eV) to our DATZ-C-CASPT2 VDE, we arrived at our best estimate of VDE (i.e., 1.106 eV). This value is in excellent agreement with the experimental VDE recorded in this work (i.e., 1.11 eV). At the same composite theoretical approach, an AEA energy of 1.055 eV is predicted for NdF_2.

Under the MRCI and MRCI+Q levels of theory, we have calculated 39 excited electronic states of NdF_2 that span within 0−0.85 eV. Our excited state findings are listed in the ESI Table S6. The complexity of this system is clearly demonstrated by its closely arranged electronic states. For example, NdF_2 populated 13 electronic states within 0−0.1 eV and another 13 electronic states from 0.16 to 0.27 eV. All these 26 electronic states of NdF_2 possess dominant $4f^36s^1$ electron configurations. All remaining electronic states (0.68−0.85 eV) investigated in the present work displayed $4f^35d^1$ electron configurations (ESI Table S6). As mentioned before, the spin−orbit effects are crucial for gaining more accurate findings for lanthanide-based systems and critically important for reaching experimental harmony. Our spin−orbit effect accounted MRCI+Q vertical excitation energies of NdF_2 and corresponding VDEs of NdF_2^- are given in Figure S2. Our calculations predicted two main sets of VDEs around the 1.11−1.26 eV and 1.38−1.49 eV regions (Figure S1) and these align well with the two main spectral features of the photoelectron spectrum (i.e., 1.11 and 1.42 eV).

CONCLUSION

In summary, this study presents a detailed characterization of the NdF_2 molecule and its anion using anion photoelectron spectroscopy in conjunction with multireference quantum chemical methods. The electronic structure of NdF_2 is revealed to be highly multireference in nature, with a dense set of low-energy excited states that underscore the challenges in modeling lanthanide systems. In addition, discussion of the similarities in molecular structure between that of analogous UF_2 substantiates the idea of periodicity among the chemical elements.

ASSOCIATED CONTENT

Supporting Information

The Supporting Information is available free of charge at https://pubs.acs.org/doi/10.1021/acs.jpca.6c01401.

Optimized geometries, vibrational frequencies, and relative energies of NdF_2 and NdF_2^- across multiple spin states, calculated at the DFT and CASPT2 levels. Vertical detachment and excitation energies from various theoretical approaches are also included. Figures include the anion photoelectron spectrum (aPES) of $^{150}NdF_2^-$ and computed spin−orbit detachment energies (PDF)

https://doi.org/10.1021/acs.jpca.6c01401
J. Phys. Chem. A XXXX, XXX, XXX−XXX

AUTHOR INFORMATION

Corresponding Authors

Kit H. Bowen − *Department of Chemistry, Johns Hopkins University, Baltimore, Maryland 21218, United States;* orcid.org/0000-0002-2858-6352; Email: kbowen@jhu.edu

Isuru R. Ariyarathna − *Theoretical Division, Los Alamos National Laboratory, Los Alamos, New Mexico 87545, United States*; Email: isuru@lanl.gov

Authors

Burak A. Tufekci − *Department of Chemistry, Johns Hopkins University, Baltimore, Maryland 21218, United States;* orcid.org/0000-0002-6964-6630

Kathryn Foreman − *Department of Chemistry, Johns Hopkins University, Baltimore, Maryland 21218, United States;* orcid.org/0000-0002-7388-8165

Complete contact information is available at: https://pubs.acs.org/10.1021/acs.jpca.6c01401

Author Contributions

B.A.T. and I.A. contributed equally to this work and are joint first authors. B.A.T. and K.F. completed the experimental work, and I.A. completed the computational work. K.H.B. supervised the experimental part of the work.

Notes

The authors declare no competing financial interest.

ACKNOWLEDGMENTS

The experimental material herein is based upon work supported by the U.S. Department of Energy (DOE), Office of Science, Office of Basic Energy Sciences, Heavy Element Chemistry Program under award number DE-SC0022977 (K.H.B.). The support of the Los Alamos National Laboratory (LANL) Laboratory Directed Research and Development program, Project No. 20240737PRD1, is acknowledged. This research used resources provided by the Los Alamos National Laboratory Institutional Computing Program, which is supported by the U.S. Department of Energy National Nuclear Security Administration under Contract No. 89233218CNA000001.

REFERENCES

(1) Murty, Y. V.; Alvin, M. A.; Lifton Jack, P.; Eds.; *Rare Earth Metals and Minerals Industries: status and Prospects*; Cham: Springer International Publishing. 2024.

(2) Nkiawete, M. M.; Vander Wal, R. L. Rare Earth Elements: Sector Allocations and Supply Chain Considerations. *J. Rare Earths* **2025**, *43* (1), 1−8.

(3) Spedding, F. H. The Rare Earths. *Sci. Am* **1951**, *185* (5), 26−31.

(4) Sun, C.; Xu, Q.; Xiao, Y.; Yang, Y. Electrochemical Deposition of Nd and Nd−Fe Alloy from Cu6Nd Alloy in a NaCl−KCl−NdCl3Melt. *Int. J. Miner. Metall. Mater.* **2020**, *27* (12), 1650−1656.

(5) Huang, C.; Liu, X.; Gao, Y.; Liu, S.; Li, B. Cathodic Processes of Neodymium(III) in LiF−NdF_3−Nd_2O_3 Melts. *Faraday Discuss* **2016**, *190*, 339−349.

(6) Hamel, C.; Chamelot, P.; Taxil, P. Neodymium(III) Cathodic Processes in Molten Fluorides. *Electrochim. Acta* **2004**, *49* (25), 4467−4476.

(7) Yuan, Q.; Lu, X.; Takeda, O.; Zhu, H. Influence of Fluoride Ions on Electrochemical Behavior of Lanthanum and Neodymium Ions in Molten LiCl. *Electrochemistry* **2024**, *92* (6), 063001.

(8) Cotton, S. *Lanthanide and Actinide Chemistry*, 1st ed.; Wiley, 2006. .

(9) Bart, S. C. What Is the "Lanthanide Contraction"? *Inorg. Chem.* **2023**, *62* (9), 3713−3714.

(10) Li, Z.; Binnemans, K. Hydration Counteracts the Separation of Lanthanides by Solvent Extraction. *AIChE J.* **2020**, *66* (9), No. e16545.

(11) Higgins, R. F.; Ruoff, K. P.; Kumar, A.; Schelter, E. J. Coordination Chemistry-Driven Approaches to Rare Earth Element Separations. *Acc. Chem. Res.* **2022**, *55* (18), 2616−2627.

(12) Wang, S. G.; Schwarz, W. H. E. Lanthanide Diatomics and Lanthanide Contractions. *J. Phys. Chem.* **1995**, *99* (30), 11687−11695.

(13) Li, W.-L.; Hu, H.-S.; Jian, T.; Lopez, G. V.; Su, J.; Li, J.; Wang, L.-S. Probing the Electronic Structures of Low Oxidation-State Uranium Fluoride Molecules UF x − (x = 2−4). *J. Chem. Phys.* **2013**, *139* (24), 244303.

(14) Gerhards, M.; Thomas, O. C.; Nilles, J. M.; Zheng, W.-J.; Bowen, K. H. Cobalt−Benzene Cluster Anions: Mass Spectrometry and Negative Ion Photoelectron Spectroscopy. *J. Chem. Phys.* **2002**, *116* (23), 10247−10252.

(15) Chen, X.; Ning, C. Accurate Electron Affinity of Pb and Isotope Shifts of Binding Energies of Pb−. *J. Chem. Phys.* **2016**, *145* (8), 084303.

(16) Stephens, P. J.; Devlin, F. J.; Chabalowski, C. F.; Frisch, M. J. Ab Initio Calculation of Vibrational Absorption and Circular Dichroism Spectra Using Density Functional Force Fields. *J. Phys. Chem.* **1994**, *98* (45), 11623−11627.

(17) Becke, A. D. D.-F. T., III. The Role of Exact Exchange. *J. Chem. Phys.* **1993**, *98* (7), 5648−5652.

(18) Kendall, R. A.; Dunning, T. H.; Harrison, R. J. Electron Affinities of the First-Row Atoms Revisited. Systematic Basis Sets and Wave Functions. *J. Chem. Phys.* **1992**, *96* (9), 6796−6806.

(19) Dolg, M.; Stoll, H.; Preuss, H. Energy-Adjusted *a b i n i t i o* Pseudopotentials for the Rare Earth Elements. *J. Chem. Phys.* **1989**, *90* (3), 1730−1734.

(20) Cao, X.; Dolg, M. Segmented Contraction Scheme for Small-Core Lanthanide Pseudopotential Basis Sets. *J. Mol. Struct. Theochem.* **2002**, *581* (1−3), 139−147.

(21) Werner, H.-J.; Knowles, P. J.; Manby, F. R.; Black, J. A.; Doll, K.; Heßelmann, A.; Kats, D.; Köhn, A.; Korona, T.; Kreplin, D. A.; Ma, Q.; Miller, T. F.; Mitrushchenkov, A.; Peterson, K. A.; Polyak, I.; Rauhut, G.; Sibaev, M. The Molpro Quantum Chemistry Package. *J. Chem. Phys.* **2020**, *152* (14), 144107.

(22) Werner, H.; Knowles, P. J.; Knizia, G.; Manby, F. R.; Schütz, M. Molpro: A General-purpose Quantum Chemistry Program Package. *Wiley Interdiscip. Rev.: Comput. Mol. Sci.* **2012**, *2* (2), 242−253.

(23) Lu, Q.; Peterson, K. A. Correlation Consistent Basis Sets for Lanthanides: The Atoms La−Lu. *J. Chem. Phys.* **2016**, *145* (5), 054111.

(24) De Jong, W. A.; Harrison, R. J.; Dixon, D. A. Parallel Douglas−Kroll Energy and Gradients in NWChem: Estimating Scalar Relativistic Effects Using Douglas−Kroll Contracted Basis Sets. *J. Chem. Phys.* **2001**, *114* (1), 48−53.

(25) Dunning, T. H. Gaussian Basis Sets for Use in Correlated Molecular Calculations. I. The Atoms Boron through Neon and Hydrogen. *J. Chem. Phys.* **1989**, *90* (2), 1007−1023.

(26) Pritchard, B. P.; Altarawy, D.; Didier, B.; Gibson, T. D.; Windus, T. L. New Basis Set Exchange: An Open, Up-to-Date Resource for the Molecular Sciences Community. *J. Chem. Inf. Model* **2019**, *59* (11), 4814−4820.

(27) Woon, D. E.; Dunning, T. H. Gaussian Basis Sets for Use in Correlated Molecular Calculations. IV. Calculation of Static Electrical Response Properties. *J. Chem. Phys.* **1994**, *100* (4), 2975−2988.

(28) Knowles, P. J.; Werner, H.-J. An Efficient Method for the Evaluation of Coupling Coefficients in Configuration Interaction Calculations. *Chem. Phys. Lett.* **1988**, *145* (6), 514−522.

(29) Werner, H.-J.; Knowles, P. J. An Efficient Internally Contracted Multiconfiguration−Reference Configuration Interaction Method. *J. Chem. Phys.* **1988**, *89* (9), 5803−5814.
(30) Shamasundar, K. R.; Knizia, G.; Werner, H.-J. A New Internally Contracted Multi-Reference Configuration Interaction Method. *J. Chem. Phys.* **2011**, *135* (5), 054101.
(31) Langhoff, S. R.; Davidson, E. R. Configuration Interaction Calculations on the Nitrogen Molecule. *Int. J. Quantum Chem.* **1974**, *8* (1), 61−72.
(32) Knowles, P. J.; Werner, H.-J. An Efficient Second-Order MC SCF Method for Long Configuration Expansions. *Chem. Phys. Lett.* **1985**, *115* (3), 259−267.
(33) Werner, H.-J.; Knowles, P. J. A Second Order Multiconfiguration SCF Procedure with Optimum Convergence. *J. Chem. Phys.* **1985**, *82* (11), 5053−5063.
(34) Kreplin, D. A.; Knowles, P. J.; Werner, H.-J. Second-Order MCSCF Optimization Revisited. I. Improved Algorithms for Fast and Robust Second-Order CASSCF Convergence. *J. Chem. Phys.* **2019**, *150* (19), 194106.
(35) Kreplin, D. A.; Knowles, P. J.; Werner, H.-J. Combined First- and Second-MCSCF Optimization Revisited. II. Order Orbital Optimization for Large Molecules. *J. Chem. Phys.* **2020**, *152* (7), 074102.
(36) Knizia, G. Intrinsic Atomic Orbitals: An Unbiased Bridge between Quantum Theory and Chemical Concepts. *J. Chem. Theory Comput.* **2013**, *9* (11), 4834−4843.

https://doi.org/10.1021/acs.jpca.6c01401
J. Phys. Chem. A XXXX, XXX, XXX−XXX